

# Local to Global Normalization Dynamic by Nonlinear Local Interactions

Matthias S. Keil\*

*Basic Psychology Department, Faculty for Psychology, University of Barcelona (UB),  
Passeig de la Vall d'Hebron 171, E-08035 Barcelona (Spain)*

(Dated: November 20, 2018)

Here, I present a novel method for normalizing a finite set of numbers, which is studied by the domain of biological vision. Normalizing in this context means searching the maximum and minimum number in a set and then rescaling all numbers such that they fit into a numerical interval. My method computes the minimum and maximum number by two pseudo-diffusion processes in separate diffusion layers. Activity of these layers feed into a third layer for performing the rescaling operation. The dynamic of the network is richer than merely performing a rescaling of its input, and reveals phenomena like contrast detection, contrast enhancement, and a transient compression of the numerical range of the input. Apart from presenting computer simulations, some properties of the diffusion operators and the network are analyzed mathematically. Furthermore, a method is proposed for to freeze the model's state when adaptation is observed.

PACS numbers: 84.35.+i, 87.18.Bb, 87.18.Hf, 87.18.Sn, 87.19.Dd, 89.75.Kd

Keywords: Adaptation, normalization, diffusion, network

## I. INTRODUCTION

What is the difference between adaptation and normalization? Are these just two distinct processes, or can they be related? The purpose of this paper is to develop a model whose dynamic smoothly proceeds from local adaptation to global normalization. Mathematical properties of the model are analyzed, and its dynamical properties are evaluated with luminance images. I study the model within the framework of biological vision, where emphasis is laid on understanding the emergence of adaptation within the model's dynamic. Finally, a method is proposed for freezing the dynamic at the moment when adaptation occurs. But to begin with, I briefly describe how adaptation and normalization contribute to information processing in the brain.

Adaptation refers to the adjustment of a sense organ to the intensity or quality of stimulation [1]. There is agreement that adaptation is important for the function of nervous systems, since without corresponding mechanisms any given neuron with its limited dynamic range would stay silent or operate in saturation most of the time [2]. When considering a population of *cells* (e.g. formal processing units or biological neurons), then adaptation is usually understood as a locally acting process, which can be carried out independently for individual cells or groups of cells, respectively (e.g., individual photoreceptors [3, 4, 5] vs. groups of photoreceptors[6, 7]). Thus, adaptation refers to sensitivity adjustment of output signals as a function of input signals.

Normalization on the other hand usually refers to establishing standardized conditions for one or more qualities. For example, at some stage in the brain, the retinal image may have been normalized with respect to illumination

conditions, such that each face or object is represented to have similar illumination patterns, and subsequent recognition stages work in a more robust fashion. Or, once a face image has been detected by an artificial face recognition system, it can be normalized with respect to head tilt or head rotation. In this way a standardized candidate face is obtained, which facilitates matching it to other standardized faces from a database.

Normalization is also used for describing the establishment of standardized conditions for a population of neurons. In this context, normalization processes usually act as gain control mechanisms. For instance, Grossberg [8] proposed “shunting competitive networks” (in his terms) for accurate signal processing in the presence of noise to avoid the noise-saturation dilemma. Because neurons have a fixed input range, weak signals get masked by noise, and neurons' signal only the noisy fluctuations in the input signal. On the other hand, strong signals cause neurons to saturate, and any variations within the input cannot be distinguished. Shunting networks implement the multiplicative relationship between membrane voltages of neurons and conductance changes that are caused by network input on the one hand and signals on the other. This multiplicative relationship acts as a gain control mechanism that enables these networks to automatically re-tune their sensitivity in response to fluctuating background inputs. As Grossberg demonstrated [8], such networks exhibit a normalization property in the sense that the total (or pooled) activity of all neurons is independent of the number of neurons. Along these lines, Heeger and co-workers proposed a normalization model to account for the observed non-linearities with the cortical simple cell responses, such as response saturation and cross-orientation inhibition [9, 10, 11]. Similar to Grossberg's “shunting competitive networks”, in Heeger's model a neuron's output activity is adjusted by the pooled activity of a population of many other neurons (“normalization pool”). This “normalization pool”

---

\*Electronic address: matsATcvc.uab.es; threequarksATyahoo.com; AT=@

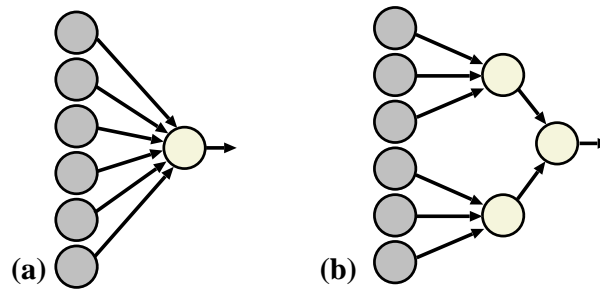


FIG. 1: **Possible network structures for extracting minimum or maximum activities of cells.** Each of the networks shown in this figure are supposed to select the maximum (or minimum) activity value among the leftmost units. The selected maximum (or minimum) is available at the rightmost unit. **(a)** Two-layer network with global connectivity pattern. **(b)** Three-layer network which extracts in its second layer the (local) maximum of the units to which it is connected. The rightmost unit subsequently selects from these local maximum the global one.

exerts divisive inhibition on the response of a target neuron, and in this way it acts as a gain control mechanism for that cell.

The circuit models proposed by Grossberg and Heeger describe how responses of a group of neurons can be normalized. Both methods rely on the interaction of some target neuron with a number of surrounding neurons. The interaction is brought about by hard-wiring the target neurons with surrounding neurons. In contrast, the normalization scheme introduced in this paper is based on diffusion mechanisms, and thus interactions only take place between adjacent cells. Specifically, within the scope of the present paper, normalization is understood as mapping a set of numbers with finite but in principle arbitrary numerical range onto a fixed target range (below we will see that non-trivial features like contrast enhancement and adaptation phenomena emerge from a network which implements this normalization mechanism).

Whereas in Grossberg’s scheme the normalization process renders the total activity of a group of cells independent of the number of cells ([8]), with my definition of normalization it is clear that in most cases the activity summed over all cells will depend on their number. A further difference concerns the implementation of activity bounds. In Grossberg’s scheme, reversal potentials establish an upper (lower) bound on the activity of each cell which can be reached by excitation (inhibition). However, the highest activity value of the normalized cell population depends on the activity of all other cells (as the total activity is constant). In other words, one cannot rely on the presence of distinguished activity values as it is the case in my approach. In a normalized population of my approach there is always at least one cell which has zero activity, and at least one cell with activity one. The usual proceeding for normalizing a set of numbers can be subdivided into two successive stages. First, the maximum and the minimum members of the set are determined. These two values are then used in a second stage for re-scaling all set elements such that after re-scaling the elements fall into a pre-defined numerical interval (or numerical range).

If we wish to design a corresponding algorithm for the first stage of the just described process (i.e. finding the maximum and the minimum), we would have to employ two memories for storing the *current* (i.e., a local) maximum and minimum, and compare these values successively with all remaining set elements. After we finished with comparing, the memory would contain the *global* maximum and minimum. Because every set member has to interact explicitly with the memories, the whole process is said to involve global operations. The global nature is mirrored in the connection structure of a correspondingly designed network. Figure 1(a) shows a schematic drawing of such a network, where one distinguished network unit shares connections with all the others. This unit is supposed to represent the maximum (or minimum) activity value of the set of units to which it is connected to. Due to its global connectivity, however, our network seems not to be a very plausible candidate for a “biologically” model, because (biological) neurons are known to interact in a more local fashion. This implausibility can be relaxed by proposing an alternative connectivity pattern (figure 1(b)).

Nevertheless, the two units representing the maximum and the minimum, respectively, need to interact subsequently again with the input units, in order to put into effect the re-scaling operation that implements the gain control mechanism. This means that one would require yet another set of non-local connections, analogously to the pattern shown in figure 1. This led me to the question whether such normalization can be achieved in a more “biological” or local fashion, or even by employing only interactions between adjacent network units. Presuming the existence of corresponding mechanisms, one has to explore in addition whether they could, in principle, be carried out by nerve cells in a biophysically plausible way. Below I present a network (the *dynamical normalization network*), which achieves normalization by means of lateral propagation of activity between adjacent network cells. To this end, parameterized diffusion operators were developed. In their limit cases, these operators implement non-linear and non-conservative diffusion processes

(“pseudo-diffusion”). The dynamic of pseudo-diffusion proceeds from local to global in a continuous fashion, without utilizing any connectivity structure apart from coupling among nearest neighbors.

The dynamic normalization network consists of a total of four layers: an input layer, two diffusion layers, and the normalization or output layer, where all layers interact. Numerical simulations with luminance images revealed that the dynamic of the normalization layer is functionally more rich than just performing a re-scaling of its input. Initially, the dynamic reveals contrast enhancement similar to high-pass filtering.

Furthermore, under certain conditions, an adaptation phenomenon (“dynamic compression”) can be observed in the initial phase of the dynamic. As it is described in detail below (section III B), the strength of the dynamic compression effect depends on the size of high activity regions in the input, and their relative positions with respect to other local maxima.

## II. FORMAL DESCRIPTION OF NONLINEAR DIFFUSION

The dynamic normalization network is based on nonlinear diffusion operators. In order to proof some of their properties, it is necessary that the nonlinear diffusion operators are differentiable. Accordingly, we define at first an operator  $\mathcal{T}_\lambda[\cdot]$  which is parameterized over  $\lambda$  as

$$\mathcal{T}_\lambda[x] = \frac{\eta x}{1 + e^{-\lambda x}} \quad (1)$$

where  $\eta$  is a normalization constant that is defined as

$$\eta = 1 + e^{-|\lambda|}. \quad (2)$$

Through the specific choice of  $\lambda$ , we can “steer” the operator  $\mathcal{T}_\lambda[\cdot]$  continuously from linearity ( $\mathcal{T}_0 \equiv \mathcal{T}_{\lambda=0}$ )

$$\lambda = 0 \rightsquigarrow \mathcal{T}_0[x] = x \quad (3)$$

to half wave rectification (i.e. selection of the maximum between zero and its argument)

$$\lim_{\lambda \rightarrow +\infty} \mathcal{T}_\lambda[x] \equiv \max(x, 0) \quad (4)$$

or inverse half wave rectification (i.e. selection of the minimum between zero and its argument)

$$\lim_{\lambda \rightarrow -\infty} \mathcal{T}_\lambda[x] \equiv \min(0, x). \quad (5)$$

Notice that the operator satisfies  $T_{-\infty}[-x] = -T_{+\infty}[x]$ .

### A. Spatially continuous nonlinear diffusion equation in one dimension

With the operator  $\mathcal{T}_\lambda[\cdot]$ , one can define a general diffusion scheme which contains heat-diffusion as a special

case for  $\lambda = 0$ . To this end, consider, without loss of generality, the general form of a diffusion equation for a quantity  $f(x, t)$  (here referred to as “activity”)

$$\frac{\partial f(x)}{\partial t} = \frac{\partial}{\partial x} \left( D(x) \frac{\partial f}{\partial x} \right) \quad (6)$$

where  $D(x) \geq 0$  is the diffusion coefficient. If  $D(x)$  depends on  $x$ , then the last equation describes a nonlinear diffusion process, otherwise ordinary heat diffusion. Consequently, by applying the operator  $\mathcal{T}_\lambda[\cdot]$  on the gradients, the following *pseudo-diffusion* process is obtained (which reduces to heat diffusion for  $\lambda = 0$ ):

$$\frac{\partial f(x)}{\partial t} = \frac{\partial}{\partial x} \left( D(x) \mathcal{T}_\lambda \left[ \frac{\partial f}{\partial x} \right] \right). \quad (7)$$

By defining  $z(x) \equiv \partial f(x)/\partial x$  and differencing we obtain

$$\frac{\partial f(x)}{\partial t} = \frac{\partial D(x)}{\partial x} \mathcal{T}_\lambda[z] + D(x) \frac{\partial \mathcal{T}_\lambda[z]}{\partial z} \frac{\partial z(x)}{\partial x}. \quad (8)$$

If  $D(x) = D = \text{const.}$ , the last equation reduces to

$$\frac{\partial f(x)}{\partial t} = D \frac{\partial \mathcal{T}_\lambda[z]}{\partial z} \frac{\partial^2 f(x)}{\partial x^2}. \quad (9)$$

The last equation looks in fact like an ordinary diffusion equation if we consider the factor  $D \partial \mathcal{T}_\lambda[z]/\partial z$  as an “effective diffusion coefficient”. But which effect has the derivative  $\partial \mathcal{T}_\lambda[z]/\partial z$ ? In appendix B it is shown that it approximates a Heaviside (or step) function  $H$  for  $\lim_{\lambda \rightarrow +\infty}$ , that is

$$\lim_{\lambda \rightarrow +\infty} \frac{\partial \mathcal{T}_\lambda[z]}{\partial z} \approx H(z). \quad (10)$$

In analogy to the previous case it can be shown that

$$\lim_{\lambda \rightarrow -\infty} \frac{\partial \mathcal{T}_\lambda[z]}{\partial z} \approx -H(z). \quad (11)$$

For a given cell,  $\lambda$  specifies the ratio between negative and positive influx into the cell from its neighbors. Consider the case  $\lambda \rightarrow \infty$  for a cell at position  $x$ . If the activity of any adjacent cell is higher, then the gradient  $z(x) \equiv \partial f(x)/\partial x$  will be positive and an influx of activity to cell  $x$  takes place, because in equation 8 the pseudo-diffusion term  $\partial z(x)/\partial x$  is multiplied by one as a consequence of equation 10. Equation 10 also implies that any negative gradient at  $x$  will make the pseudo-diffusion term be multiplied by zero, and thus prevents an influx of negative activity into cell  $x$ . The essence of this mechanism is that activity at  $x$  can only increase until any gradient has dissipated. As an alternative, this mechanism may be understood as an auto-adaptive diffusion constant which regulates its value according to the current gradient at  $x$  (figure 2).

For  $\lambda \rightarrow -\infty$  the mechanism works just vice versa, and the activity for a cell at position  $x$  may only decrease. The linear (or heat) diffusion equation is obtained for  $\lambda = 0$ , where both a positive-valued and a negative-valued influx can enter the cell.

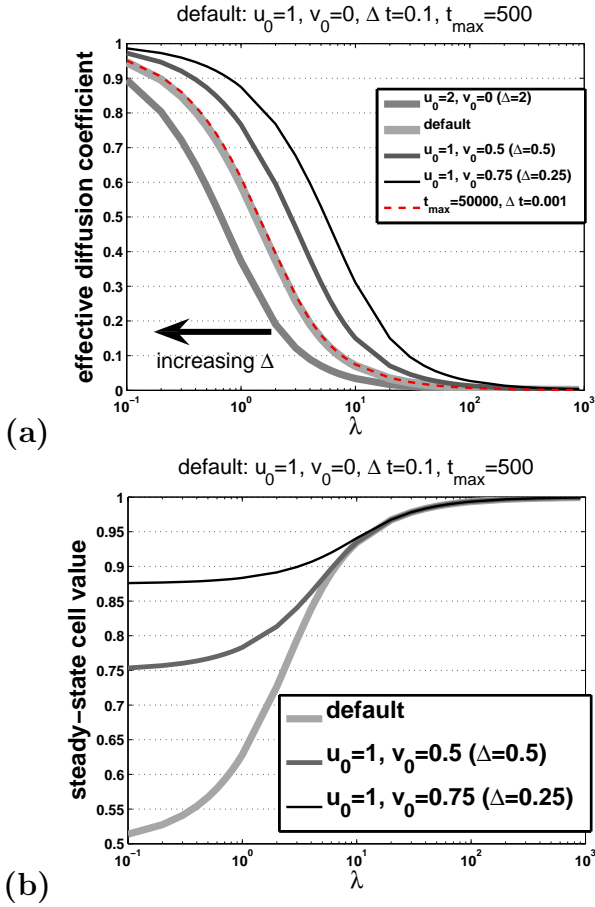


FIG. 2: **Diffusion for  $0 \leq \lambda < \infty$ .** (a) The plot relates  $\lambda$  of equation 12 (ordinate) to the effective diffusion constant  $\gamma$  of equation 13 (abscissa). The different curves relate to different simulation parameters as indicated in the legend. Parameters that do not appear in the legend correspond to default values as indicated in the figure heading ( $\Delta t = 0.1$  integration step size,  $t_{\max} = 500$  iteration limit). An increase of the value of the gradient  $\Delta \equiv u_0 - v_0$  at  $t = 0$  makes the curves  $\gamma(\lambda)$  shift to the left (arrow). With  $\Delta t = 0.1$  or smaller, results do not depend in a significant way on integration step size (dashed line which overlaps with the curve for the default case). With increasing increments  $\Delta t$ , however, all solid lines displace to the left by the same amount. (b) The steady-state cell values  $u_\infty \equiv v_\infty$  as a function of  $\lambda$  show a sigmoidal relationship which smoothly passes from heat diffusion ( $u_\infty \equiv [u_0 + v_0]/2$  for  $\lambda = 0$ ) to implementing a maximum operation ( $u_\infty \equiv \max[u_0, v_0]$  for  $\lambda = \infty$ ).

### B. Intermediate values of $\lambda$ for a two cell system

Intermediate values of  $\lambda$  attenuate either negative ( $\lambda > 0$ ) or positive influx ( $\lambda < 0$ ). The amount of attenuation depends on  $\lambda$ . To illustrate, consider a simplified pseudo-diffusion system which consists only of two cells  $u(t)$  and

$v(t)$ :

$$\frac{\partial u}{\partial t} = \mathcal{T}_\lambda[v - u] \quad (12)$$

$$\frac{\partial v}{\partial t} = \mathcal{T}_\lambda[u - v]$$

Furthermore, we define the following *surrogate* system

$$\frac{\partial a}{\partial t} = \gamma(b - a) \quad (13)$$

$$\frac{\partial b}{\partial t} = a - b$$

with a diffusion coefficient  $\gamma$ . Note that because diffusion coefficients are different for  $a(t)$  and  $b(t)$  (that is,  $\gamma$  and 1, respectively), the last equation implements a non-linear diffusion system. Without loss of generality, we assume  $\lambda > 0$ , and  $u_0 - v_0 > 0$  at  $t = 0$ . Furthermore, let both diffusion systems have the same initial conditions  $u_0 = a_0$  and  $b_0 = v_0$ . With this configuration of parameters, the influx into cell  $u$  is negative, and will be attenuated because of  $\lambda > 0$ . Dependent on the precise value of  $\lambda$ , the steady-state values of  $u_\infty$  and  $v_\infty$  will be situated somewhere between  $(u_0 + v_0)/2$  for  $\lambda = 0$ , or  $\max(u_0, v_0)$  for  $\lambda \rightarrow +\infty$ . Now, to understand the behavior for  $0 < \lambda < \infty$ , the diffusion coefficient  $\gamma$  is (numerically) determined such that both diffusion systems (equations 12 and 13) have the same equilibrium state, that is  $u_\infty = a_\infty$  and  $v_\infty = b_\infty$  (and also  $u_\infty = v_\infty$ ).

With the assumptions  $\lambda > 0$  and  $u_0 - v_0 > 0$ , it follows that  $\gamma < 1$ , because in order to obtain the same steady-state values for both diffusion systems, the negative influx into cell  $a$  needs to be attenuated. Figure 2a shows that in this case the effective diffusion coefficient  $\gamma$  and  $\lambda$  have a sigmoidal relationship. The sigmoid shifts to the left as a function of  $\Delta \equiv u_0 - v_0$  (or equivalently  $a_0 - b_0$ ).

Figure 2b shows that steady-state values as a function of  $\lambda$  also follow a sigmoidal relationship. Cell values at convergence smoothly pass from heat diffusion ( $u_\infty \equiv [u_0 + v_0]/2$  for  $\lambda = 0$ ) to implementing a maximum operation ( $u_\infty \equiv \max[u_0, v_0]$  for  $\lambda = \infty$ ). Analogous considerations hold for negative values of  $\lambda$ .

### C. Spatially discrete pseudo-diffusion equation in two dimensions

Based on a centered finite difference representation of the Laplacian operator, we define a parameterized diffusion operator acting on a function  $f(x, y)$  as

$$\begin{aligned} \mathcal{K}_\lambda f(x, y) = & \mathcal{T}_\lambda [f(x+1, y) - f(x, y)] \\ & + \mathcal{T}_\lambda [f(x-1, y) - f(x, y)] \\ & + \mathcal{T}_\lambda [f(x, y+1) - f(x, y)] \\ & + \mathcal{T}_\lambda [f(x, y-1) - f(x, y)] \end{aligned} \quad (14)$$

where a grid spacing of  $\Delta x = \Delta y = 1$  is assumed. We will make use of the following compact notation

$$\mathcal{K}_{+\infty} \equiv \lim_{\lambda \rightarrow +\infty} \mathcal{K}_\lambda \quad (15)$$

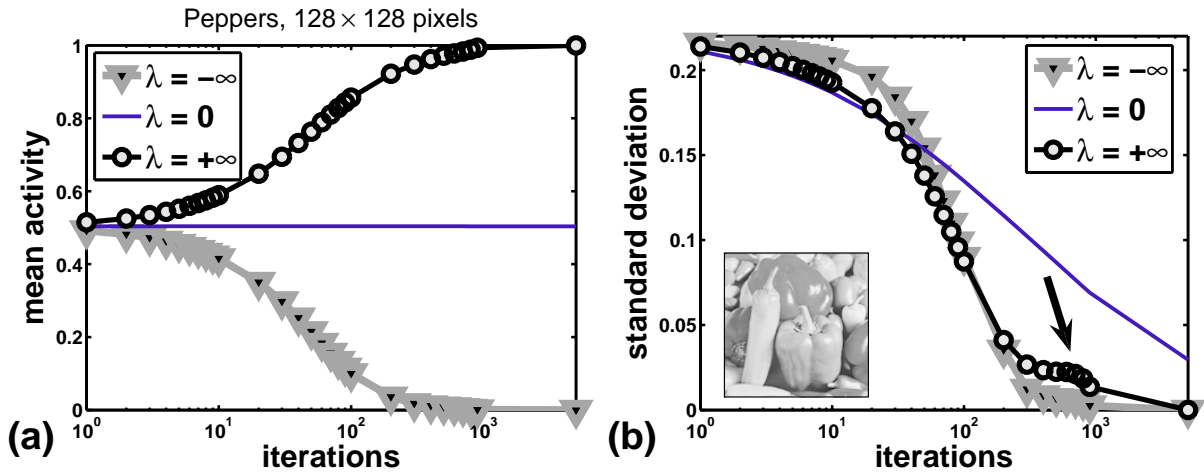


FIG. 3: **Pseudo-diffusion converges faster than heat diffusion (Peppers image)**. Curves show the temporal evolution of the mean activity together with standard deviations for heat diffusion “ $\lambda = 0$ ” (no symbols, eq. 17), max-diffusion “ $\lambda = +\infty$ ” (circles, eq. 20), and min-diffusion “ $\lambda = -\infty$ ” (triangles, eq. 19). For computing the mean activity, averaging took place over all values of the respective (pseudo-) diffusion layer. The **Peppers** image ( $0 \leq s_{ij} \leq 1$ , size  $128 \times 128$  pixels, inset) defined the initial state of each layer. **(a)** Mean activity remains constant with time with heat diffusion (heat diffusion is conservative), but approaches the minimum (maximum) value of  $s$  in the min-diffusion layer (max-diffusion layer). **(b)** The minimum (maximum) is finally adopted by all cells  $a_{ij}$  ( $b_{ij}$ ), as indicated by decreasing standard deviations. Compared to heat diffusion, the pseudo-diffusion systems converge in fewer simulation time steps to a uniform state, but for their simulation more computations per time step are needed (cf. equation 1). Moreover, pseudo-diffusion does not converge after  $2 \cdot 128$  iterations (the largest distance between two cells on a  $N \times N$  grid is  $2N$  in a Manhattan architecture). A single iteration is insufficient to propagate a maximum from one cell to the next, as all diffusion operators are normalized by the number of adjacent cells (in addition,  $D\Delta t \leq 1/2$ , see section A). Note further that standard deviation of the max-diffusion layer has a local maximum (arrow). This at first sight paradoxical effect is explained with figure 4.

and

$$\mathcal{K}_{-\infty} \equiv \lim_{\lambda \rightarrow -\infty} \mathcal{K}_{\lambda}. \quad (16)$$

Note that  $\mathcal{K}_{\lambda=0} \approx \nabla^2$  from equation 3.

In order to formulate a spatially discrete pseudo-diffusion scheme, we consider a diffusion layer (i.e. a finite grid on which diffusion takes place) with an equal number  $N$  of rows  $i$  and columns  $j$ , that is  $1 \leq i, j \leq N$ . We use a discrete-in-space and continuous-in-time notation, where  $f_{ij} = f(j, i)$ ,  $f_{i,j+1} = f(j+1, i)$  and so on [12]. With the above definitions, heat diffusion is described as:

$$\frac{\partial f_{ij}}{\partial t} = D \cdot \mathcal{K}_0 f_{ij}(t) \quad (17)$$

where  $D = \text{const.}$  is the diffusion coefficient. The process is assumed to start at time  $t = t_0$  with the initial condition  $f_{ij}(t_0) = s_{ij}$ . From now on we assume that the  $s_{ij}$  represent an intensity or luminance distribution (i.e., “ $s$  represents a gray level image”). Since diffusion takes place in a bounded domain (i.e. we have a finite number  $N \times N$  of grid points), and we also use adiabatic boundary conditions (i.e. there is neither inward flux nor any flux outward over the domain boundary, i.e.  $\partial f_{ij}/\partial t = 0$  for  $(i, j) \in \{(i, 0), (i, N), (0, j), (N, j)\}$ ) [13], the total activity described by equation 17 does not depend on time

(figure 3), that is

$$\sum_{i,j}^N f_{ij}(t) = \text{const.} \quad (18)$$

The last expression expresses that diffusion is conservative – activity is neither created nor destroyed. Although the 2-D heat diffusion equation cannot create new activity levels which have not already been present at time  $t_0$  [14], it can create extrema in activity domains that have a dimension greater than one (cf. [15], p.532). A *min-diffusion layer* will eventually compute the minimum of all values and is defined as:

$$\frac{\partial a_{ij}}{\partial t} = D \cdot \mathcal{K}_{-\infty} a_{ij}(t). \quad (19)$$

A *max-diffusion layer* will eventually compute the maximum of all values and is defined as:

$$\frac{\partial b_{ij}}{\partial t} = D \cdot \mathcal{K}_{+\infty} b_{ij}(t). \quad (20)$$

We assume equal initial conditions  $a_{ij}(t_0) = b_{ij}(t_0) = s_{ij}$  for the min-diffusion layer and the max-diffusion layer at time  $t = t_0$ .

Whereas equation 17 preserves its total activity, the min-diffusion layer and max-diffusion layer, respectively, do

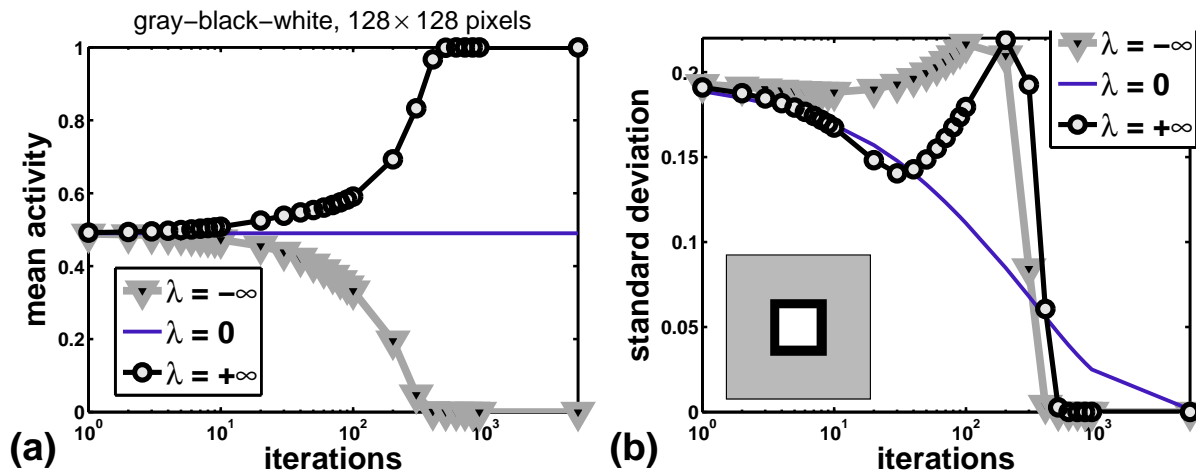


FIG. 4: **Why standard deviations can increase with pseudo-diffusion.** Standard deviations of the min-diffusion layer and the max-diffusion layer reach a local or global maximum if at some time in the layers a configuration is obtained which consists of two domains with each domain having a different activity level (similar to a luminance step). Of course, a necessary precondition is that the initially provided configuration (here three domains with gray  $s_{ij} = 0.5$ , black  $s_{ij} = 0$ , and white  $s_{ij} = 1$ , see inset) has a smaller standard deviation than the “step”-like configuration which is generated as an intermediate state. In the max-diffusion layer, for example, a step-like configuration is reached as soon as the black frame is dissolved from both sides (i.e., “eaten” by the gray and the white region). The effect depends on luminance levels and the relative amount of black, white, and gray. It can be also obtained for different layouts of the regions (e.g., gray-white-black or black-gray-white).

not. The total activity of the min-diffusion layer decreases with time and converges to (figure 3)

$$\lim_{t \rightarrow \infty} \sum_{i,j} a_{ij}(t) = N^2 \min_{i,j} \{s_{ij}\}. \quad (21)$$

The total activity of the max-diffusion layer increases with time and converges to (figure 3)

$$\lim_{t \rightarrow \infty} \sum_{i,j} b_{ij}(t) = N^2 \max_{i,j} \{s_{ij}\}. \quad (22)$$

In other words, all cells  $a_{ij}$  of the min-diffusion layer will finally contain the global minimum of the input  $s_{ij}$

$$A := \min_{i,j} \{s_{ij}\} = \lim_{t \rightarrow \infty} a_{ij}(t) \quad \forall i, j \quad (23)$$

and all cells  $b_{ij}$  of the max-diffusion layer will end up with the global maximum

$$B := \max_{i,j} \{s_{ij}\} = \lim_{t \rightarrow \infty} b_{ij}(t) \quad \forall i, j. \quad (24)$$

This can be explained as follows. A cell  $a_{ij}$  of the min-diffusion layer may only *decrease* its activity from one time step to the next, until any activity gradient between  $a_{ij}$  and its nearest neighbors has dissipated. As a consequence,  $a_{ij}$  adopts the minimum activity value of the neighborhood, including itself. Because the last arguments apply to *all* cells  $a_{ij}$ , eventually all cells will adopt the minimum activity  $\min_{i,j} \{s_{ij}\}$  at convergence. Convergence occurs if  $a_{ij} = a_{kl} \forall (i, j), (k, l)$  (i.e. when

no more activity gradient exists). The dynamic of the process is illustrated by figure 5.

In an analogous way, in the diffusion process described by the max-diffusion layer, all cells  $b_{ij}$  could only *increase* their activity, given the existence of any activity gradient. If any cell has a maximum activity value, then finally all cells will adopt this maximum, since only then all gradients have dissipated.

Hence, both nonlinear diffusion systems are non-conservative, because they do not fulfill requirements analogous to equation 18.

### III. DYNAMIC NORMALIZATION BY NEXT NEIGHBOR INTERACTIONS

Equipped with the pseudo-diffusion operators defined in the last section, we are now ready to define the *dynamic normalization* network. The network normalizes a given input  $s_{ij}$  with respect to numerical range, but without taking resort to any global memory for determining the minimum and maximum. Rather, the global minimum and maximum are computed in the min-diffusion layer and the max-diffusion layer, respectively, by only exchanging information between adjacent cells.

We start with the following linear scaling scheme, which is typically used for normalizing a fixed set of numbers (again, see introduction):

$$c_{ij} = \frac{s_{ij} - a_{ij}}{b_{ij} - a_{ij}} \quad \text{where } 1 \leq i, j \leq N. \quad (25)$$

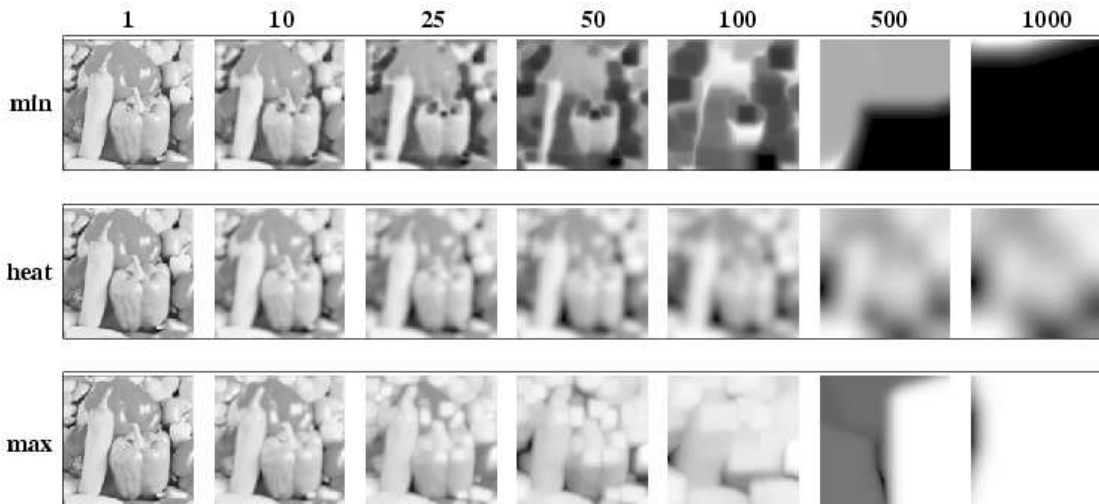


FIG. 5: **Snapshots of diffusion states.** Images show snapshots of max-diffusion ( $a_{ij}$ , first row), heat diffusion ( $f_{ij}$ , middle row), and min-diffusion ( $b_{ij}$ , last row) for the **Peppers** image (size  $128 \times 128$  pixels). The numbers indicate elapsed iterations. Whereas heat diffusion just blurs the image, min-diffusion and max-diffusion create “islands” corresponding to local minima and maxima, respectively. With increasing time, islands decrease in number and increase in size, until eventually a single island occupies the whole region. Then, the min-diffusion layer and the max-diffusion layer have eventually computed the global minimum and maximum, respectively. Due to our boundary conditions (see methods), diffusion is faster at domain boundaries (see section A). Brighter gray levels correspond to higher cell activities.

Because of equation 23 and 24 the variable  $c_{ij}$  will contain (after a sufficiently long time) a normalized representation of  $s_{ij}$ , that is

$$s_{ij} \in [A, B] \mapsto c_{ij} \in [0, 1] \quad (26)$$

( $A$  and  $B$  are the global minimum and maximum, respectively, of  $\{s_{ij}\}$ ). To arrive at a fully dynamical system, we formally interpret equation 25 as the steady-state solution of

$$\frac{\partial c_{ij}}{\partial t} = b_{ij}(0 - c_{ij}) - a_{ij}(1 - c_{ij}) + s_{ij} \quad (27)$$

which shall be called *dynamic normalization*. Notice that by using dynamic normalization we naturally avoid the singularity of equation 25 that occurs for  $b_{ij} = a_{ij}$ .

Figure 6 visualizes the state of equation 27 at different time steps. Initially, the dynamic normalization process is similar to high-pass filtering (figure 7), what can be explained as follows. Contrasts are abrupt changes in luminance. Consider a luminance change from dark to bright. Then, the dark side has a local minimum, and the bright side a local maximum, which propagates in the min-diffusion layer and the max-diffusion layer, respectively (figure 5). When the local minimum (maximum) has propagated to the position of the bright (dark) side of the step, then the bright (dark) side will be normalized to one (zero). As the dynamic continues to evolve, local maxima and minima propagate further, thereby “eating” (i.e., annihilating) other smaller local maxima and minima. In figure 6, this annihilation of local maxima and minima, respectively, is visible through a gradual filling-in of image structures from the boundaries. A normalized version of the original image is finally obtained when

$\partial c_{ij}/\partial t = 0$ . Depending on (i) how small the  $s_{ij}$  are, and (ii) the choice of integration step size  $\Delta t$ , the steady-state of  $c_{ij}$  can be reached with delay compared to the steady-states of  $a_{ij}$  and  $b_{ij}$ , respectively. This is now examined in more detail.

#### A. Time to convergence for dynamic normalization

Figure 8 shows the relationship between the time to convergence and the numerical range of the input  $s_{ij}$ : the smaller the  $s_{ij}$ , the more iterations are necessary to accomplish the mapping expressed by equation 26. Mathematically, this can be seen as follows. Assume that a general solution of equation 27 has the form

$$c_{ij}(t) = C_0 e^{-t/\tau} + C_1 \quad (28)$$

where  $C_0$  and  $C_1$  are constants which are defined by the initial conditions, and  $\tau$  is a time constant. Plugging the last equation into equation 27 yields

$$C_0 e^{-t/\tau} \left[ b_{ij} - a_{ij} - \frac{1}{\tau} \right] = -C_1 (b_{ij} - a_{ij}) + s_{ij} - a_{ij} \quad (29)$$

By identifying

$$\tau = \tau_{ij}(t) \equiv \frac{1}{b_{ij}(t) - a_{ij}(t)} \quad (30)$$

we obtain

$$C_1 = \frac{s_{ij} - a_{ij}}{b_{ij} - a_{ij}}, \quad (31)$$



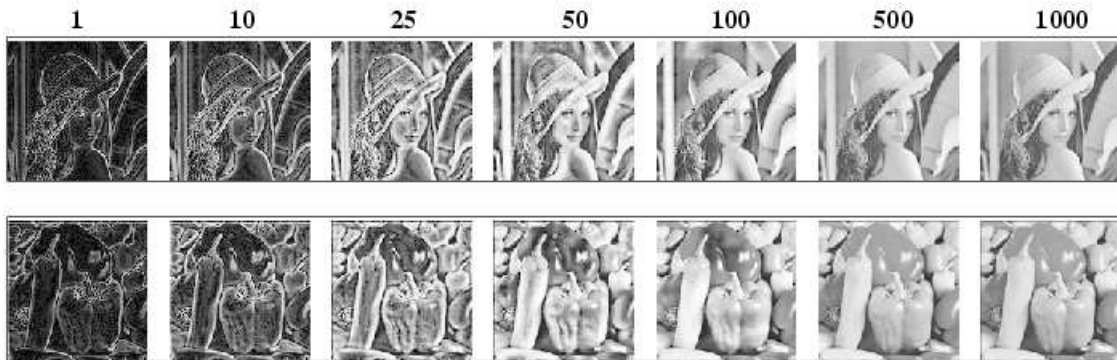


FIG. 6: **Snapshots of dynamic normalization.** The images show equation 27 at different time steps (indicated by the numbers) for images (size  $128 \times 128$  pixels) **Lena** (top row) and **Peppers** (bottom row). The dynamic begins similar to high-pass filtering (cf. figure 7), proceeds with contrast enhancement and “fills in” image structures from their contrast contours, until finally a normalized version of the input image is obtained. Brighter gray levels indicate higher cell activities. In order to improve visualization, images were rescaled individually.

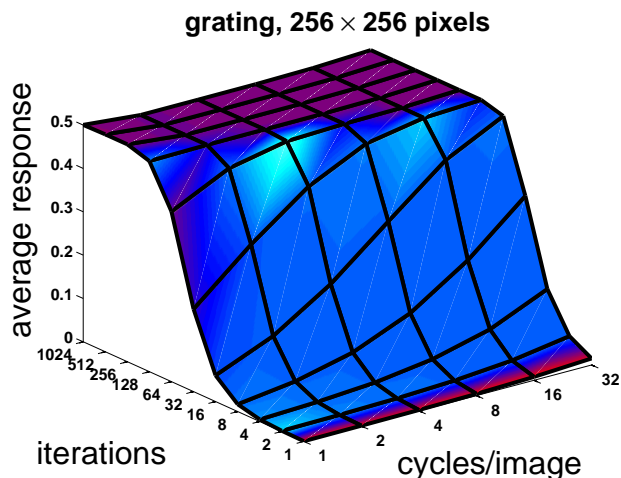


FIG. 7: **Spatial frequency vs. time for a sine wave grating.** This experiment is analogous to figure 8(b), but here for a sine wave grating (size  $256 \times 256$  pixels). At each time, the graphs show the maximum activity value of equation 27. Obviously, at a fixed number of iterations ( $\lesssim 64$ ), the dynamic normalization network’s signal transmission characteristics is high-pass. No frequency selectivity is observed after convergence ( $\gtrsim 128$  iterations).

and from the initial condition  $c_{ij}(t=0) = 0 \quad \forall i, j$  we furthermore get  $C_0 = -C_1$ , which finally gives the solution

$$c_{ij}(t) = \frac{s_{ij} - a_{ij}}{b_{ij} - a_{ij}} \left( 1 - e^{-t/\tau_{ij}} \right). \quad (32)$$

On grounds of the definition of  $\tau$  (equation 30) we obtain two insights.

First, since the time constant  $\tau$  of the dynamic normalization process is a function of both  $a_{ij}(t)$  and  $b_{ij}(t)$ , it is not really a constant, but rather depends on time and space because of equation 19 and 20, respectively. However,  $\tau$  can be approximated by recalling that  $a_{ij}(t)$  and

$b_{ij}(t)$  converge in time and space to the global minimum  $A$  and global maximum  $B$ , respectively, of the input  $s_{ij}$  (equation 23 and 24). Thus,  $\tau \approx 1/(B - A)$ . This leads to the second insight: the smaller are  $A$  and  $B$ , the longer it takes dynamic normalization to converge to a steady state. Or, otherwise expressed, the smaller  $\tau$  is, the faster the system converges.

Notice that when using the steady-state solution (equation 25) of dynamic normalization instead of the full dynamic process (equation 27), no dependency on input contrast is revealed, and the dependence on spatial frequency structure of the input is much weaker.

## B. Transient adaptation or dynamic compression

The dynamic normalization layer reveals distinct dynamic phases. In the initial phase, image contrasts are extracted. Contrast enhancement occurs in a subsequent phase. In the final phase, the activity distribution in the dynamic normalization layer is just a re-scaled version of the input. In a second phase between the initial and the final phase, one observes adaptation: image structures with substantially different light intensities in the input are mapped to a smaller range of activities in the dynamic normalization layer. This effect is the *dynamic range compression*. For its illustration an input image was subdivided into four quadrants (“contrast tiles”, figure 9). Each of the tiles has a different range of luminance values. Because the available tonal range for displaying the tiled image is too small to match the range of all tiles, some of the image details in the darker tiles are displayed in black. Nevertheless, a part of these details are rendered visible in the dynamic normalization layer at around 100 iterations (top row in figure 9), implying that cell activities in this layer have less dynamic range than in the input. The compression effect is quantized in figure 10, where each curve represent the mean activity and the maximum activity, respectively, of all cells of one



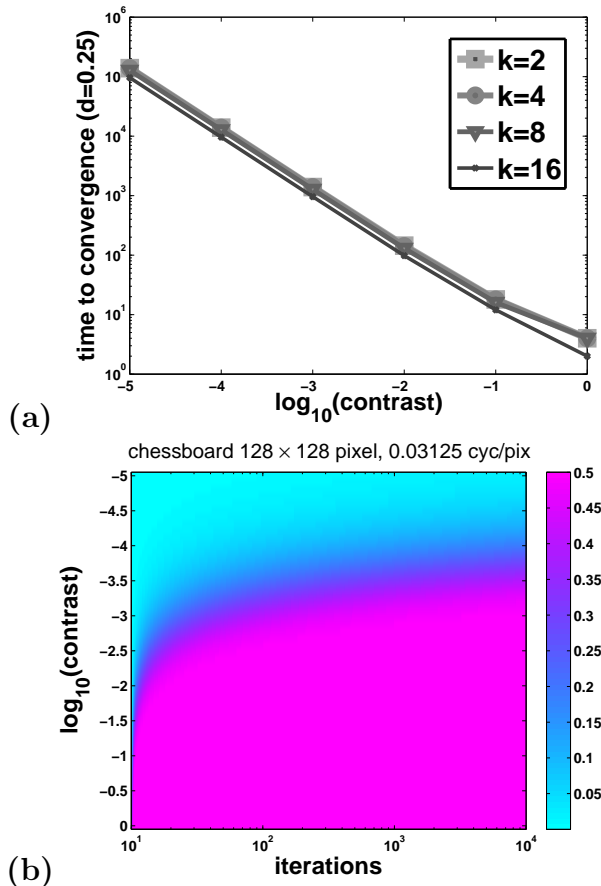


FIG. 8: **Time to convergence.** Both of the graphs show simulation results of the dynamic normalization process with a chessboard image as input (size  $128 \times 128$  pixels). For both graphs, “convergence” was defined as soon as the average activity of all cells in the dynamic normalization layer reached  $d = 0.25$  (note that at full normalization  $d = 0.5$ ). (a) Time to convergence of the dynamic normalization process depends in the first place on luminance contrast, and to a lesser extent on spatial frequency content of the input (legend: chessboard spatial frequency  $k$  in cycles per image) – curves for different spatial frequencies are similar. The simulation results are therefore consistent with equation 30. Chessboard contrast was set to the values indicated on the abscissa:  $s_{ij} \in [0, B]$  with  $B \in \{10^{-5}, 10^{-4}, 10^{-3}, 10^{-2}, 10^{-1}, 10^0\}$ . (b) Mean activity of the dynamic normalization layers is indicated by colors (inset: colorbar) as a function of iterations (abscissa) and luminance contrast (ordinate) of the chessboard image (4 cycles per image). The dynamic of the normalization process reveals a sigmoidal behavior which consists of a plateau with low activity (top, turquoise), a relatively short rising phase (blue), and a plateau with high activity (pink, bottom), where convergence has occurred.

the four tiles. The curves approach each other at around 100 iterations. Thus, the output of the dynamic normalization network can be encoded with a smaller than the original numerical range.

Figure 11 illustrates the mechanism which underlies dynamic compression. A necessary condition for dynamic

compression to occur is that the global maximum propagates with finite speed in the max-diffusion layer, and that it is spatially separated from image structures that have less dynamic range (= local maxima). When the global maxima has not yet propagated to the local maxima, then image structures are normalized by their “own” local maxima. Since normalization rescales all cell activities to the same target range (all image structures normalize to one), local normalization implies a reduction of the dynamic range. However, local maxima are annihilated as the global maximum propagates, and image structures are now getting normalized by the global maximum. Then, the entire dynamic range of the input image is recovered in the normalization layer, and dynamic range compression is abolished. The recovery of the original dynamic range can be seen when the entropy curves of figure 12(b) reduce to the entropy of the input image at  $\approx 1000$  iterations (dashed horizontal line).

### C. Process entropy

Figure 12(b) shows entropy as a function of time computed over the dynamic normalization layer. The entropy reaches a maximum in the time window where dynamic compression occurs. Notice that this maximum in entropy exceeds the entropy of the input image (dashed horizontal line). Because entropy quantifies the degree of flatness of a histogram (or probability distribution), the observed entropy maximum implies that cell activities of the dynamic normalization layer are more homogeneously distributed across the histogram than luminance values of the input. Figure 13 shows how the distribution of activities evolve over time. Initially, cell activities in the dynamic normalization layer are small, and tend to cluster around a single spot in the histogram (the cropped “hot spot” in the upper left corner of the histogram). Emanating from this “hot spot”, values start to occupy nearly the entire histogram. It is just then when an observer who is monitoring the output of the dynamic normalization network gathers the highest information about the input image.

In the consecutive part of the dynamic, the values are redistributed again in a way that they concentrate around four principal stripes. These stripes correspond to the four contrast tiles. Therefore, dynamic range compression is compatible with adaptation, since adaptation maximizes the transfer of information [18].

### D. Adaptation-by-entropy-maximisation

When computing the Shannon entropy of the output of the dynamic normalization network [17], one observes an entropy maximum at the dynamic compression effect (figure 12 and 13). Hence, a straightforward algorithm for the adaptation of images is to stop the dynamic normalization process when an entropy maximum is reached

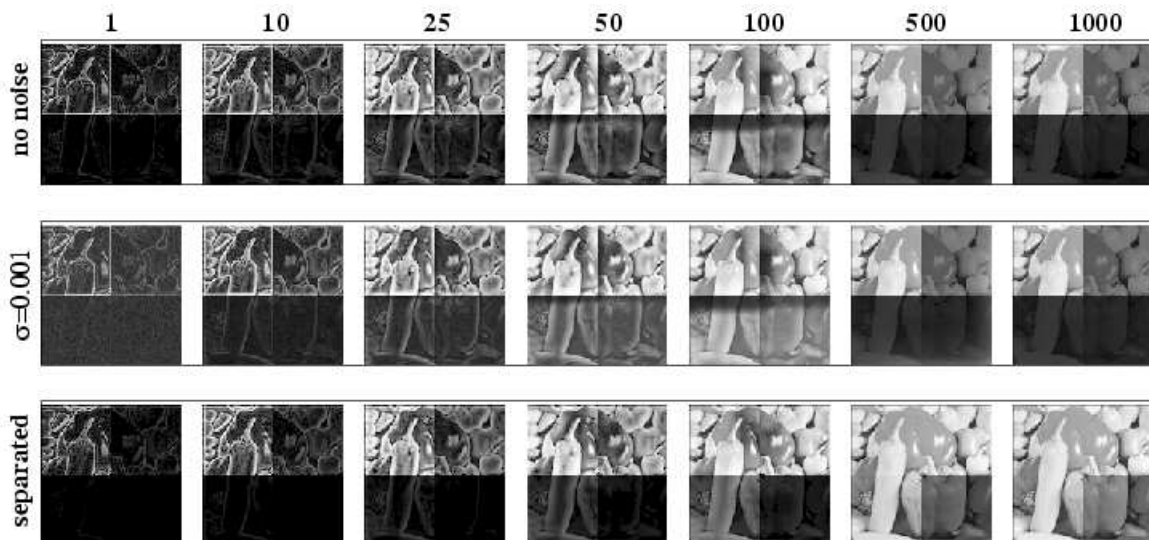


FIG. 9: **Dynamic compression.** Same as figure 6, but here for a “contrast-tiled” version of **Peppers**. Contrast-tiling means that the original image (entropy 8 bits, tiled image  $\gtrsim 14$  bits, see figure 12(a)) was subdivided in quadrants (“tiles”) to obtain the dynamic range of luminance values found in a typical outdoor scene (values were taken from [16], table 1). At an intermediate number of iterations (around 100), dynamic range compression occurs, where details in the darker tiles get better visible. **Top row:** Noise-free dynamic - compare with figure 10. The input image is shown as inset in figure 10(b). **Middle row:** Dynamic for additive Gaussian noise (see section III E 1) with standard deviation  $\sigma = 0.001$  and zero mean - see also figure 16). Obviously, moderate levels of noise improve dynamic compression and thus the visibility of the darker tiles. **Bottom row:** The tiles were disconnected from each other (i.e. no diffusion could take place across different contrast tiles), and the dynamic normalization mechanism now treats each tile as a separate image. Notice that in the first two rows all four tiles are connected (i.e., the tiles are treated as a single image), and activity propagates between tiles (as it is visible by a black shadow in the lower tiles at around 100 iterations).

(“one feedback loop”). To further enhance the dynamic compression effect, the output at the entropy maximum can be taken again as input to the dynamic normalization network, and once again we can let the dynamic normalization process continue until it reaches a maximum of entropy (“two feedback loops”). The entropy across 10 feedback loops of the just described algorithm is illustrated in figure 14 with the curve designated by “process entropy”. Figure 15 shows the output images obtained for one, two, three and 20 feedback loops. With increasing number of feedback loops, luminance information is suppressed, while contrasts are enhanced. At around 20 loops, one obtains an image which seems to contain only contours, but iterating further enhances also noise and leaves one with an image without any recognizable structures. Figure 14 shows that entropy decreases with increasing number of feedback loops (each data point is the entropy of the output at the indicated number of feedback loops). For the “tiled” and the “4th power” **Peppers** image, the entropy versus feedback loops has a maximum. Concluding, in terms of entropy, but also by visual inspection, a small number of feedback loops (one or two) seems optimal for the proposed adaptation algorithm. The algorithm should be understood as a “proof-of-concept” rather than a definite tool for image processing, because it occasionally develops artifacts. For example, future versions could address the suppression of the

dark zone which emanates from the tiles of the “tiled” **Peppers** image.

### E. Sensitivity of dynamic normalization for noise

One may argue that an adaptive mechanism designed in a way suggested by dynamic normalization is highly sensitive to noise, because it is based on the computation of minimum and maximum operations. To address this issue, we further distinguish between static noise (i.e. an offset added to the input  $s_{ij}$  which does not vary with time), and dynamic noise (i.e. an offset added to each layer which varies with time). For the first case we presume the existence of a noise-free input pattern, to which static noise is added. A worst case scenario is on hand if a couple of cells  $s_{ij}$  have high activities due to noise (“noisy cells”) which lead to an undesired increase of the true dynamic range of the input. If a read-out mechanism for the dynamic normalization layer had only the same dynamic range as the input, then the noise would obscure the relevant information of the input at convergence. Nevertheless, if there were only a few noisy cells in the input layer, then the dynamic compression effect could mitigate the worst case scenario to some extent. To assess the robustness of dynamic normalization against temporally varying noise, numerical experiments

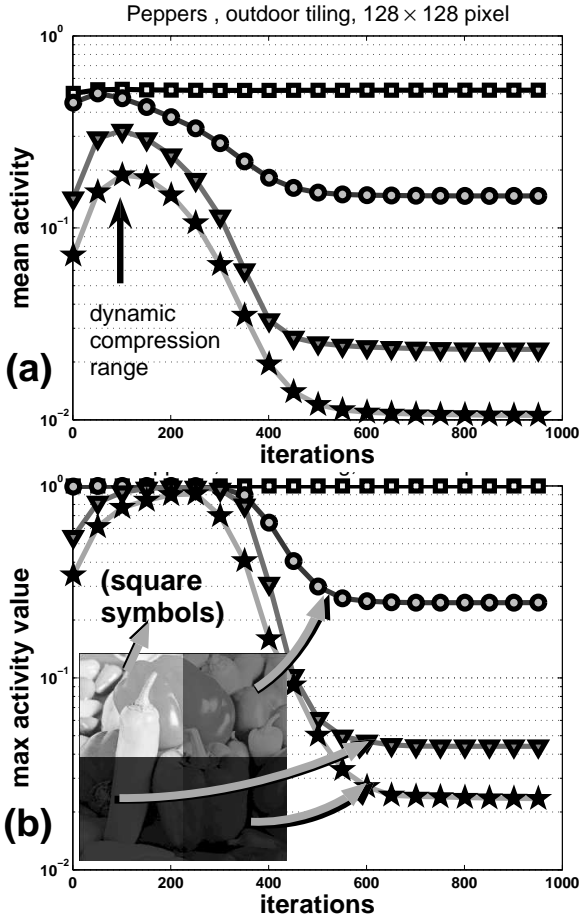


FIG. 10: **Dynamic compression of input range.** Each curve quantifies the activity across one of the four tiles (inset) of the dynamic shown in the top row of figure 9: (a) mean activity, and (b) maximum of activity. Within the time window where dynamic compression is seen, initially separated curves approach each other, and subsequently depart again. Other real-world images give similar results.

were conducted with additive, normal-distributed noise (“Gaussian noise”), with zero mean and standard deviation  $\sigma$ . Apart, additional simulations were conducted with multiplicative, uniform noise (“white noise”).

### 1. Additive, normal-distributed noise

Temporally fluctuating normal-distributed noise  $\xi_{ij}(t)$  was added to the equations 19, 20, 27, and the input  $s_{ij}$ , according to

$$x_{ij} \leftarrow x_{ij} + \sigma \xi_{ij}(t). \quad (33)$$

In the last equation,  $x_{ij}$  stands for one of the variables  $a_{ij}$ ,  $b_{ij}$ ,  $c_{ij}$ , and  $s_{ij}$ , respectively, and “ $\leftarrow$ ” means that the left hand side is replaced by the right hand side. The noise level is specified by  $\sigma$  (assuming zero mean), and  $\xi_{ij}(t)$  is assumed to be not correlated across time and/or

spatial positions. A luminance step ( $32 \times 32$  pixels) was used as input, with luminance value zero on the dark side (“black patch”, columns 1 to 16), and 1 on the bright side (“white patch”, columns 17 to 32). Thus, the mean activity of the noise free system should approach one at steady-state. We furthermore computed the Michelson contrast  $\mathcal{M}$  at each position  $(i, j)$  according to

$$\mathcal{M}_{ij} = \frac{c_{ij \in \text{white}} - c_{ij \in \text{black}}}{c_{ij \in \text{white}} + c_{ij \in \text{black}}} \quad (34)$$

where  $j \in \text{black}$  means  $1 \leq j \leq 16$  and  $j \in \text{white}$  means  $17 \leq j \leq 32$  (the row index runs over all positions  $1 \leq i \leq 32$ ).

Figure 17(a) shows the temporal evolution of the mean activity of  $\langle c_{ij} \rangle_{ij \in \text{white}}$  (i.e. averaged over white patch positions) for various noise levels  $\sigma$ . Sufficiently high noise levels significantly affect the convergence behavior of dynamic normalization - the response plateau which is seen in the noise-free case is no longer reached. Instead of the plateau, a maximum is approached, the amplitude of which decreases with increasing noise level. Figure 17(b) shows that a similar behavior is also seen for the averaged Michelson-contrast  $\langle \mathcal{M}_{ij} \rangle$ : The contrast between the black and the white patch decreases with increasing noise level. This implies that image structures are obscured by noise.

How does noise take influence on dynamic range compression? Three answers exist to this question, and they depend on the noise level. For relatively small noise levels ( $\sigma < 0.001$ ), no dramatic effect on dynamic compression is observed. For intermediate noise levels ( $\sigma \approx 0.001$ ), dynamic compression is enhanced (bottom row in figure 9, and figure 16). Enhancement happens because the net effect of noise is to add an offset, which “lifts” the darker patches of the tiled **Peppers** image. For higher noise levels, however, the darker patches drown in noise and image details get lost. Consequently, if the goal of dynamic normalization was adaptation, then suitable chosen noise levels would aid to enhance range compression, although this comes at the prize of reduced contrasts in regions with low activities (dark quadrants in the tiled **Peppers** image).

Notice that additive Gaussian noise can be easily counteracted by proposing additional mechanisms with low-pass characteristics, like spatial or temporal pooling of activity. Then, as long as the noise is not correlated over positions and time, it would simply average out.

### 2. Multiplicative and normally distributed noise

Multiplicative noise was applied to variables  $a_{ij}$ ,  $b_{ij}$ ,  $c_{ij}$ , and  $s_{ij}$ , respectively, according to

$$x_{ij} \leftarrow x_{ij} \cdot (1 + \eta * (\mu_{ij}(t) - 1)) \quad (35)$$

with  $0 \leq \mu_{ij}(t) \leq 1$  representing uniformly distributed noise which was uncorrelated across time and/or space.

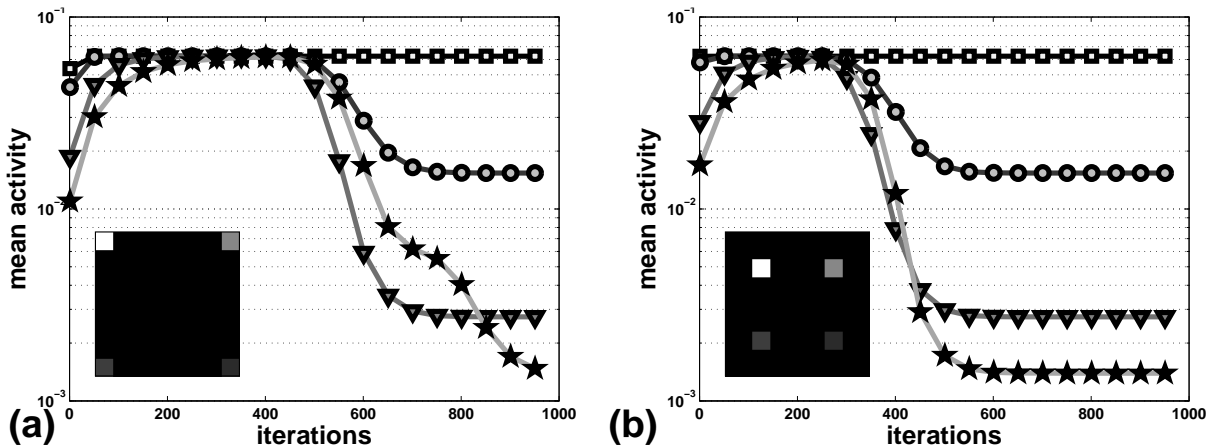


FIG. 11: **Understanding dynamic range compression.** The dynamic compression effect is a consequence of that the global maximum propagates with finite speed in the max-diffusion layer. Thus, the smaller the initial region occupied by the global maximum in the max-diffusion layer, and the greater the distance of this region from other regions of smaller cell activities or local maxima, respectively, the longer the persistence of the effect. This is illustrated with two images (insets). The images consist of zeros except for small squares with different luminance values. The global maximum corresponds to the white square ( $s = 1$ , upper left in the images). The luminance values of the squares are the same as the maximum value of each quadrant in the tiled **Peppers** image of figure 10, that is  $s = 1$ ,  $s = 0.24615$ ,  $s = 0.04385$ , and  $s = 0.02231$ , respectively. **(a)** The squares are maximally separated, and the global maximum reaches the other local maxima relatively late (mean activities were computed across the same tiles as before with the tiled **Peppers** image). As a consequence, each square is independently normalized by its local maximum until it gets invaded by a higher activity value. **(b)** Moving the four squares closer to each other goes along with a shorter duration of the dynamic compression effect. Were all four squares moved into the center of the image such that they touch each other, virtually no dynamic compression effect would be revealed, because the global maximum would instantaneously propagate to all four tiles: all local maxima would get normalized by the global maximum right off.

The noise level is specified by  $\eta \in [0, 1]$ . Dynamic normalization is not significantly affected by this type of noise, not even for  $\eta = 1$  (hence results are not shown). Multiplicative noise acts differently on maxima and minima. Maximum activities can only decrease, but never increase beyond their value in the noise free case. Therefore, no spurious maxima are introduced into the max-diffusion layer by the type of multiplicative noise considered here. On the other hand, multiplicative noise can inject spurious minima into the min-diffusion layer, if the lowest luminance value in the input image was bigger than zero. As the minimum luminance values of our images were always zero, they are consequently not affected by the multiplicative noise.

## IV. DISCUSSION

### A. Pseudo-diffusion and electrical synapses (gap junctions)

The operator  $\mathcal{K}_\lambda$  models different types of electrical synapses (gap junctions). In its linear version,  $\mathcal{K}_{\lambda=0}$  describes the exchange of both depolarizing (i.e. directed towards a neuron's firing threshold) and hyperpolarizing (i.e. directed away from a neuron's firing threshold) currents between adjacent neurons. Networks of electrically

coupled neurons are ubiquitous both in the retina (e.g. [19, 20, 21, 22, 23]) and the cortex (e.g. [24, 25, 26]). These networks can be modeled by diffusion equations (e.g. [27, 28, 29, 30]). Conversely, the operators defined by equation 15 and 16 represent models for rectifying (i.e. voltage sensitive) gap-junctions. Rectifying gap junctions were described in the crayfish (e.g. [31, 32]), and unidirectional and gated gap junctions were reported in the rat (e.g. [33]) and turtle (e.g. [33, 34]), respectively.

In organisms, rectifying gap junctions may nevertheless be implemented in a “dirty” fashion. This means that a current flux may not strictly occur in only one direction. Rather, a small amount of current may as well flow in the opposite direction. Such behavior is captured by setting  $\lambda$  to a finite value  $1 \ll |\lambda| < \infty$ , and was analyzed in figure 2.

### B. Computational aspects

Substitution of two global memories (for the minimum and the maximum activity) by two pseudo-diffusion layers of size  $N \times N$  leads to a computationally more demanding system, because more memory resources are needed and significantly more computational operations need to be carried out for their simulation. Moreover, because computation of the global maximum or minimum is

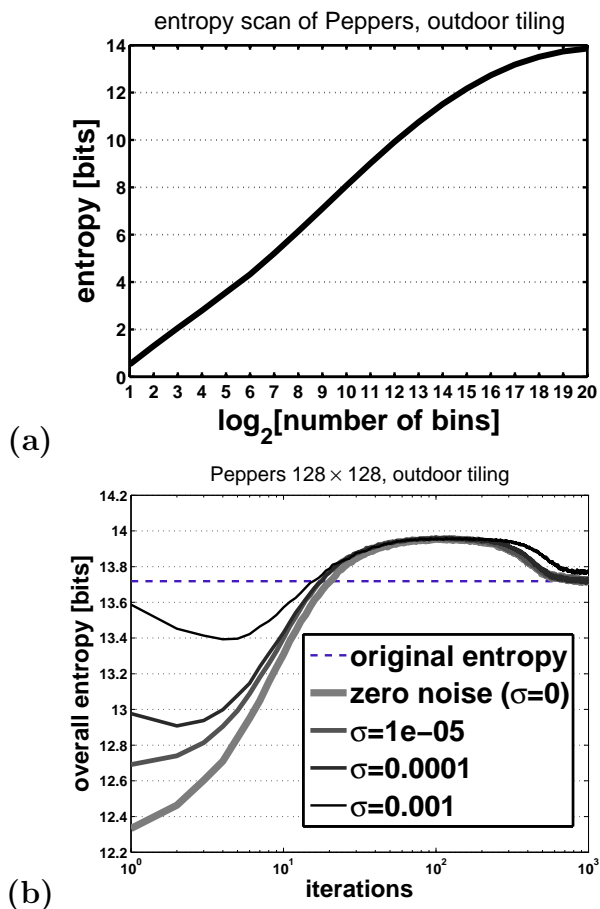


FIG. 12: **Dynamic compression, entropy and Gaussian noise.** (a) “Entropy scan” of the tiled **Peppers** image. Shannon entropy [17] was computed as a function of the number of histogram bins. The curve starts to saturate at approximately  $10^{20} = 1048576$  bins (the maximum value allowed with the computer that was used for the simulations). Thus, the entropy of the tiled image is  $\gtrsim 14$  bits. (b) Shannon entropy of the dynamic normalization layer as a function of iterations. The tiled **Peppers** image served as input. Here, hardware constraints only permitted the computation of entropy with  $15 \cdot 10^5$  bins. Each curve represents a different amount of temporally varying and normal-distributed noise (additive “Gaussian noise”) with standard deviations  $\sigma \in \{0, 10^{-5}, 10^{-4}, 10^{-3}\}$  (see inset). The dynamic compression effect is associated with plateau-like maxima in the entropy curves. The dashed horizontal line denotes the entropy of the input image.

based on local, diffusion-like interactions, a maximum or a minimum does not propagate from one cell to another from one time step to the next. The diffusion rate cannot be chosen arbitrarily high to guarantee the numerical stability of the process. The time to convergence does not only depend on the pseudo-diffusion layers reaching a steady-state, but is mainly determined by the dynamic normalization layer. The number of iterations that is needed until convergence occurs scales with the numerical range of the input. Thus, for small input values, the

number of required iterations can be quite large (see figure 8). Therefore, the dynamic normalization network cannot be seriously considered as an alternative to an ordinary normalization algorithm (i.e., searching the global maximum and minimum, and then rescaling). However, the dynamic normalization network can accomplish different tasks which cannot be accomplished with an ordinary normalization algorithm, for example detection of contrast contours, or compression of the dynamic range of the input.

## V. CONCLUSIONS

This paper introduced a parameterized diffusion operator (parameter  $\lambda$ ) and analyzed some of its properties mathematically and by computer simulations. As a special case, heat diffusion is obtained for  $\lambda = 0$ . Diffusion layers which are based on the two limit cases of the operator (for  $\lambda \rightarrow \pm\infty$ ) compute the global maximum and minimum, respectively, of the initial cell activities of the layer. This means that at convergence, all cells of the diffusion layers contain the same activity value – the maximum ( $\lambda \rightarrow \infty$ ) or the minimum ( $\lambda \rightarrow -\infty$ ). Based on these operators, a dynamic normalization network was defined (equation 27). Its steady-state solution is functionally equivalent to the ordinary rescaling of a set of numbers (equation 25), but by making the normalization process dynamic, one observes two additional properties: contrast enhancement and dynamic range compression. Both effects occur because at first normalization acts locally, similar to adaptation mechanisms. With increasing time, the normalization process gets continuously more global, until a steady-state is reached. The steady-state corresponds to a rescaling of the input in the dynamic normalization layer.

By exploiting the dynamic compression effect, it should thus be possible to design a powerful adaptation mechanism which maps an input image of an arbitrary numerical range to a smaller target range. To do so, the normalization process has to be “frozen” when dynamic compression occurs. As a first step into that direction, a simple adaptation algorithm based on the maximisation of entropy was proposed (section III D): the dynamic is frozen as soon as a maximum of entropy is reached, and the output is then fed back as new input to the dynamic normalization network. As a further improvement, the diffusion operators could be modified such that activity exchange between two cells is blocked for sufficiently large activity gradients [35]. Doing so would possibly prevent in figure 9 (first and second row) the global maximum from spreading between tiles, and would normalize each tile independently, such that ideally a dynamic similar to the bottom row in figure 9 is produced.

Systems based on pseudo-diffusion have already turned out to be of utility for a variety of purposes in image processing (for implementing filling-in mechanisms, or winner-takes all inhibition, see [35]). Pseudo-diffusion

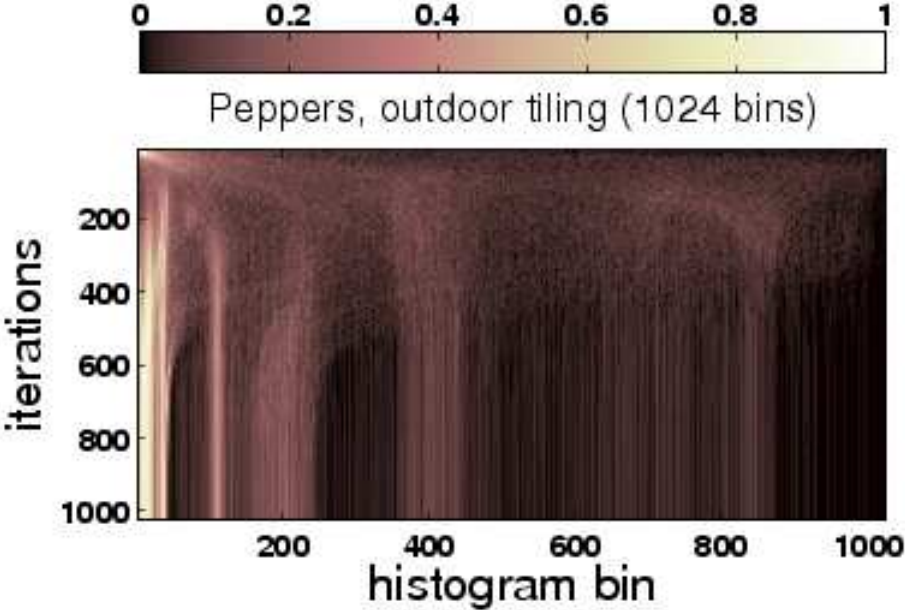


FIG. 13: **Histogram evolution of the tiled Peppers image.** Each horizontal line in the above image represents a histogram of the dynamic normalization layer (abscissa: 1024 bins per line) at a different iteration number (ordinate). Occurrence frequencies of output activity values are represented by colors (inset: colorbar).

Initially, cells in the dynamic normalization layer have small activities and concentrate in the first histogram bins (upper left corner; the first 14 time steps were dropped for visualization reasons). This highly predictable state is associated with low entropy. Immediately afterwards, values distribute themselves homogeneously over virtually all bins, and thus entropy increases. This is when dynamic compression occurs: an observer who is monitoring the output of the dynamic normalization network gathers the highest information about the input image. In other words, dynamic range compression is compatible with adaptation, since adaptation maximizes the transfer of information [18]. Subsequently values are redistributed again in a way that they concentrate along four principal stripes reflecting the four contrast tiles. This state is again associated with a lower entropy. Notice that both the way from and to the more homogeneous distribution of values is mirrored in structures similar to faint “trajectories” that sweep from left to right across the histogram.

systems can generally be used for implementing the max-operation without the need for globally acting pooling units (see for example [36] and [37]). The advantage over functionally equivalent but hardwired systems is that the region where normalization takes place can be dynamically adjusted. Furthermore, the maximum operation serves to implement invariance properties in models for object recognition (e.g. [38, 39]).

#### Acknowledgments

This work was supported by the *Juan de la Cierva* program of the Spanish government, and the the MCyT grant SEJ 2006-15095. Further support was provided by the AMOVIP INCO-DC 961646 grant from the European Community. The author likes to thank the anonymous reviewer of *Physica D* for his valuable suggestions which helped to improve the manuscript (the present version is the long version; a shorter version is to be published in

*Physica D*).

#### APPENDIX A: MATERIAL AND METHODS

All simulations were carried out using the Matlab environment (R2006b) on a Linux workstation, where both native Matlab code and mex-files programmed in C++ were used. Diffusion operators were normalized by the number of adjacent cells (normally four, along the domain boundaries three, and in the corners two). Normally, the equations describing the diffusion layers (eqs. 19 and 20), and dynamic normalization (eq. 27) turned out to be numerically stable such that a forward-time-centered-space (FTCS) Euler scheme with step size one is sufficient. (Here, we understand numerical stability such that the solution converges rather than growing in an unbounded fashion). Notice, however, the stability criterion associated with the FTCS-integration of the heat diffusion equation  $D \cdot \Delta t \leq 1/2$  (assuming grid spacing



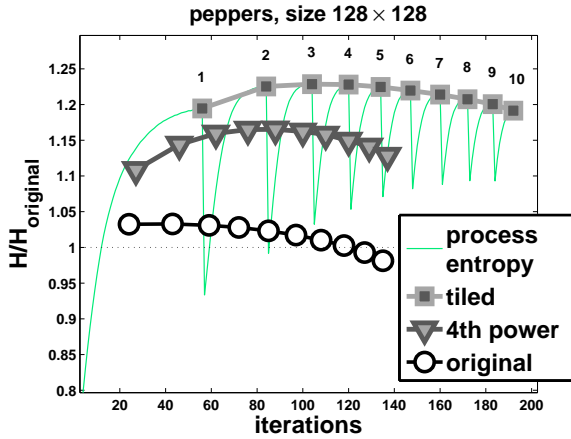


FIG. 14: **Adaptation by entropy maximisation (entropy)**. Each point of the curves “original”, “4th power”, and “tiled” corresponds to the entropy  $H$  (normalized by the entropy of each respective original image  $H_{\text{original}}$ ) at the indicated number of feedback loops of the entropy maximizing adaptation algorithm (output images at one, two, three and 20 loops are shown in the previous figure). In addition, the curve designated by “process entropy” relates the relative entropy of the full algorithm to the data points of the “tiled” Peppers image: between any two data points, the dynamic normalization network was run by using the output image at the previous data point as input until a maximum in entropy has been reached. See text for further details.

one, see section 19.2 in [40]) where  $D$  is the diffusion coefficient, and  $\Delta t$  is the integration step size. Since we compared pseudo-diffusion with Laplacian or heat diffusion (eq. 17), by default we employed Euler’s method with integration step size  $\Delta t = 0.5$  and diffusion coefficient  $D = 1$ . Exceptions are as follows. Figure 2 was simulated with  $\Delta t = 0.1$  and  $\Delta t = 0.001$ , respectively. Figure 6, 8, and figures 9 to 16 were integrated with the fourth-order Runge-Kutta method ( $\Delta t = 0.5$ ,  $D = 1$ ). For the compilation of figure 17, again the fourth-order Runge-Kutta method was used with  $\Delta t = 0.01$  and  $D = 1/\Delta t$ , to guarantee numerical stability in the presence of high noise levels.

It should be emphasized that the results presented in this paper do not depend critically on the exact value of neither  $\Delta t$  and  $D$ , nor on the specific choice of the integration method. Variation of these parameters leads to a corresponding rescaling of the time axis. Although we exemplified the behavior of the model only by means of two standard images which are commonly used for image processing (Lena and Peppers), all characteristics of the model can as well be reproduced with other images.

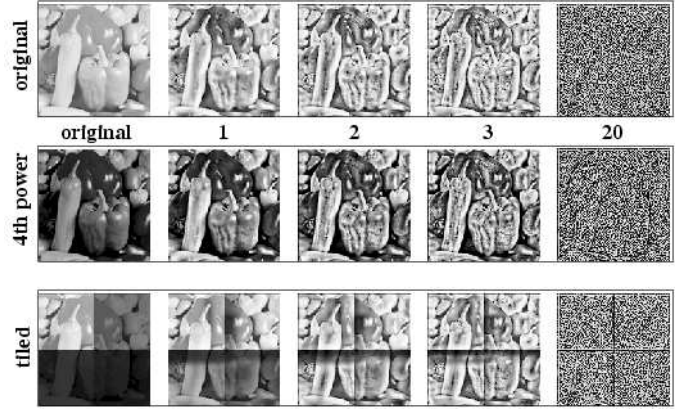


FIG. 15: **Adaptation by entropy maximisation (results)**. The first column shows the original images which were used as input to the adaptation-by-entropy-maximisation algorithm: “original” is the original pepper image; “4th power” is the original pepper images with luminance values elevated by fourth power (in this way a high-dynamic-range image is created); tiled is the tiled peppers image (cf. figure 9). The numbers designate how many feedback loops of the algorithm were run.

## APPENDIX B: PROOF OF EQUATION 10 (FOR $\lambda \rightarrow \infty$ AND $\lambda = 0$ )

Consider the derivative of the operator  $\mathcal{T}_\lambda[\cdot]$  (equation 1),

$$\frac{\partial \mathcal{T}_\lambda[z]}{\partial z} = \underbrace{\frac{\eta}{1 + e^{-\lambda z}}}_{\text{term I}} + \underbrace{\frac{\eta \lambda z e^{-\lambda z}}{(1 + e^{-\lambda z})^2}}_{\text{term II}} \quad (\text{B1})$$

where the following three cases have to be analyzed:

**Case  $\lambda = 0$ .** In this case  $\eta = 2$  from equation 2, and

$$\frac{\partial \mathcal{T}_0[z]}{\partial z} = \underbrace{\frac{\eta}{1 + 1}}_{\text{term I}} + \underbrace{0}_{\text{term II}} = 1. \quad (\text{B2})$$

Thus, for  $\lambda = 0$  the derivative is constant one for all  $z$ , and equation 7 reduces to the linear diffusion equation 6.

**Case  $\lambda \rightarrow +\infty$ .** In this case  $\eta = 1$  from equation 2, and we have to consider three additional cases according to the value of  $z$ . Note that  $z$  is treated as a constant. Hence,

$z = 0$ .

$$\lim_{\lambda \rightarrow +\infty} \frac{\partial \mathcal{T}_\lambda[z]}{\partial z} = \underbrace{\frac{\eta}{1 + 1}}_{\text{term I}} + \underbrace{0}_{\text{term II}} = \frac{1}{2}. \quad (\text{B3})$$

This is to say that if the gradient  $z$  vanishes, then the derivative is constant with value  $1/2$ .

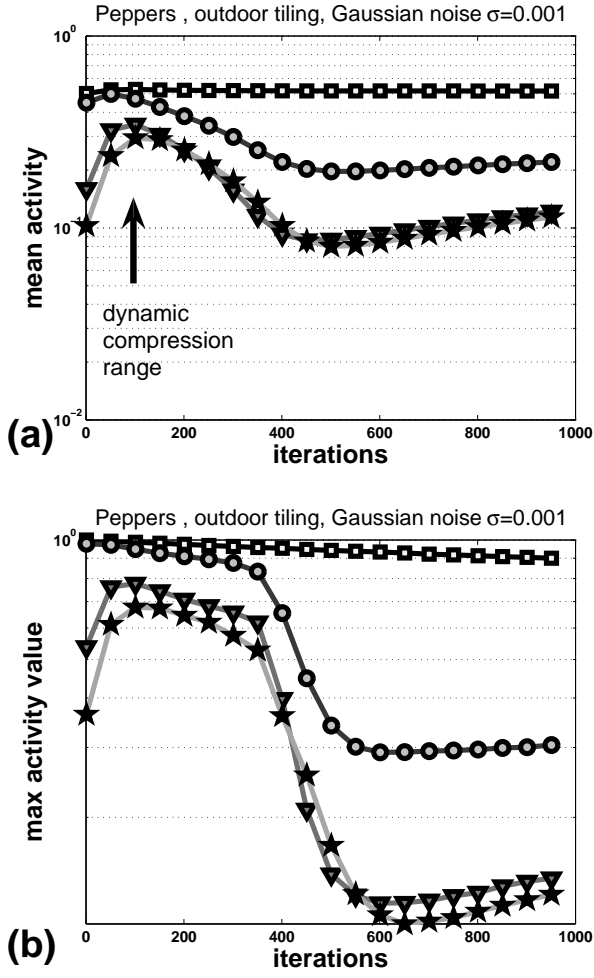


FIG. 16: **Dynamic compression in the presence of noise.** Same as figure 10, but here with additive and temporally varying Gaussian noise (standard deviation  $\sigma = 0.001$ , zero mean). Snapshots of the noisy dynamic are shown in the middle row of figure 9. Evidently, suitable chosen noise levels can enhance the dynamic compression effect. See also figure 12(b) for the dependence of entropy on noise levels.

$z > 0$ . We start with evaluating *term I* of equation B1,

$$\lim_{\lambda \rightarrow +\infty} \frac{\eta}{1 + \underbrace{e^{-\lambda|z|}}_{\rightarrow 0}} = \eta = 1 \quad (\text{term I}). \quad (\text{B4})$$

In the numerator of *term II* appears a product of the kind “ $\infty \cdot 0$ ”. One may argue that the exponential  $\exp(-\lambda|z|)$  always approaches zero much more faster than the term  $\eta\lambda|z|$  is able to grow (or one may equivalently apply l’Hôpital’s rule to this product by applying  $d/d\lambda$  on each factor),

$$\lim_{\lambda \rightarrow +\infty} \frac{(\eta\lambda|z|) \cdot (e^{-\lambda|z|})}{(1 + e^{-\lambda|z|})^2} \rightsquigarrow \lim_{\lambda \rightarrow +\infty} \frac{\overbrace{(\eta|z|)}^{\text{const.}} \cdot \overbrace{(-|z|e^{-\lambda|z|})}^{\rightarrow -0}}{\underbrace{(1 + e^{-\lambda|z|})^2}_{\rightarrow 0}} = 0 \quad (\text{term II}). \quad (\text{B5})$$

Thus, for  $\lim_{\lambda \rightarrow +\infty}$  evaluates equation B1 to 1 for all  $z > 0$ .

$z < 0$ . Evaluating *term I*,

$$\lim_{\lambda \rightarrow +\infty} \frac{\eta}{1 + \underbrace{e^{\lambda|z|}}_{\rightarrow \infty}} = 0 \quad (\text{term I}). \quad (\text{B6})$$

Evaluating *term II* (again there is a little more work to do),

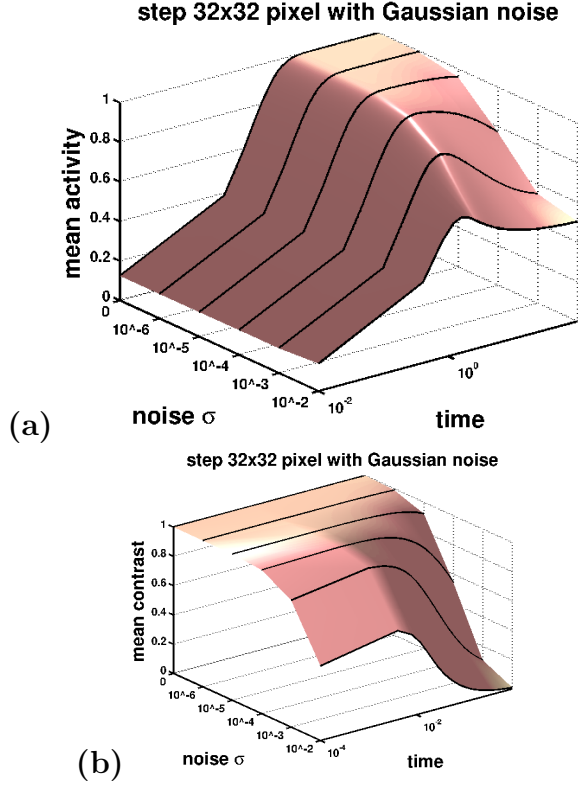


FIG. 17: **Dynamic normalization with additive Gaussian noise.** A luminance step (activities zero and one) was used to analyze the behavior of dynamic normalization network in the presence of additive and temporally varying Gaussian noise (zero mean, standard deviation  $\sigma$  as indicated in the plot). (a) Activity of dynamic normalization averaged over the cells corresponding to the white region of the luminance step. (b) Michelson contrast between the black and the white region of the step, averaged over respective positions. See text for further details.

$$\lim_{\lambda \rightarrow +\infty} \frac{-\eta\lambda|z|}{2 + e^{-\lambda|z|} + e^{\lambda|z|}} \rightsquigarrow \lim_{\lambda \rightarrow +\infty} \frac{\eta}{\underbrace{e^{-\lambda|z|}}_{\rightarrow 0} - \underbrace{e^{\lambda|z|}}_{\rightarrow \infty}} = 0 \quad (\text{term II}). \quad (\text{B7})$$

Hence, for  $\lim_{\lambda \rightarrow +\infty}$  evaluates equation B1 to 0 for all  $z < 0$ .

□

Summarizing the above we saw that equation B1 behaves approximately [41] like a Heaviside function  $H$  for  $\lim_{\lambda \rightarrow +\infty}$ , thus equation 10 is proofed. The proof of equation 11 (for  $\lambda \rightarrow \infty$ ) proceeds in straight analogy.

- [1] Merriam-Webster, Merriam-Webster Online Dictionary (16 Feb. 2007) <http://www.merriam-webster.com> (2007).  
 [2] J. Walraven, C. Enroth-Cugell, D. Hood, D. MacLeod,

- and J. Schnapf, in *Visual Perception: The Neurophysiological Foundations*, edited by L. Spillman and J. Werner (Academic Press, New York, 1990), pp. 53–101.  
 [3] G. Carpenter and S. Grossberg, *Journal of Theoretical*

- Biology **1**, 1 (1981).
- [4] H. van Hateren, *Journal of Vision* **5**, 331 (2005).
- [5] M. Keil and J. Vitrià, *EURASIP Journal on Advances in Signal Processing* **2007**, Article ID 51684, 10 pages (2007), doi:10.1155/2007/51684.
- [6] R. Gross and V. Brajovic, in *Springer Lecture Notes in Computer Sciences*, edited by J. Kittler and M. Nixon (AVBPA, 2003), vol. 2688, pp. 10–18.
- [7] S. Hong and S. Grossberg, *Neural Networks* **17**, 787 (2004).
- [8] S. Grossberg, *Behavioral and Brain Sciences* **6**, 625 (1983).
- [9] M. Carandini, D. Heeger, and J. Movshon, *The Journal of Neuroscience* **17**, 8621 (1997).
- [10] M. Carandini and D. Heeger, *Science* **264**, 1333 (1994).
- [11] D. Heeger, *Visual Neuroscience* **9**, 181 (1992).
- [12] Moving along rows corresponds to discrete  $y$ -values, and moving along columns corresponds to discrete values of  $x$ .
- [13] Adiabatic boundary conditions are implemented in the simulations by reducing the diffusion operators at the domain borders to existing neighbors.
- [14] J. Koenderink, *Biological Cybernetics* **50**, 363 (1984).
- [15] L. Lifshitz and S. Pizer, *IEEE Transactions on Pattern Analysis and Machine Intelligence* **12**, 529 (1990).
- [16] D. Jobson, Z. Rahmann, and G. Woodell, *IEEE Transactions on Image Processing* **6**, 965 (1997).
- [17] C. Shannon, *Bell Systems Technical Journal* **27**, 379 (1948).
- [18] M. Wainwright, *Vision Research* **39**, 3960 (1999).
- [19] E. Raviola and N. B. Gilula, *Journal of Cell Biology* **65**, 192 (1975).
- [20] H. Kolb, *Journal of Neurocytology* **6**, 131 (1977).
- [21] R. Nelson, T. Lynn, A. Dickinson-Nelson, and H. Kolb, in *Neurocircuitry of the Retina: A Cajal Memorial* (Elsevier, New York, 1985), pp. 109–121.
- [22] S. L. Mills and S. C. Massey, *Visual Neuroscience* **11**, 549 (1994).
- [23] S. L. Mills and S. C. Massey, *Journal of Neuroscience* **20**, 8629 (2000).
- [24] J. Gibson, M. Beierlein, and B. Connors, *Nature* **402**, 75 (1999).
- [25] M. Galarreta and S. Hestrin, *Nature* **402**, 72 (1999).
- [26] M. Galarreta and S. Hestrin, *Proceedings of the National Academy of Sciences USA* **99**, 12438 (2002).
- [27] K.-I. Naka and W. Rushton, *Journal of Physiology* **193**, 437 (1967).
- [28] T. Lamb, *Journal of Physiology* **263**, 239 (1976).
- [29] A. Winfree, in *The Handbook of Brain Theory and Neural Networks*, edited by M. Arbib (The MIT Press, Cambridge, Massachusetts, 1995), pp. 1054–1056.
- [30] J. Benda, R. Bock, P. Rujan, and J. Ammermüller, *Visual Neuroscience* **18**, 835 (2001).
- [31] D. Edwards, W. Heitler, E. Leise, and R. Friscke, *Journal of Neuroscience* **11**, 2117 (1991).
- [32] D. Edwards, S.-R. Yeh, and F. Krasne, *Proceedings of the National Academy of Sciences USA* **9**, 7145 (1998).
- [33] F. Bukauskas, A. Angele, V. Verselis, and M. Bennett, *Proceedings of the National Academy of Sciences USA* **99**, 7113 (2002).
- [34] M. Piccolino, J. Neyton, and H. Gerschenfeld, *The Journal of Neuroscience* **4**, 2477 (1984).
- [35] M. Keil, G. Cristóbal, T. Hansen, and H. Neumann, *Neural Networks* **18**, 1319 (2005).
- [36] A. Yu, M. Giese, and T. Poggio, *Neural Computation* **14**, 2857 (2002).
- [37] M. Keil, Ph.D. thesis, Universität Ulm, Faculty for Computer Science, Ulm, Germany (2003).
- [38] M. Riesenhuber and T. Poggio, *Nature Neuroscience* **2**, 1019 (1999).
- [39] M. Riesenhuber and T. Poggio, *Nature Neuroscience* **3**, 1199 (2000).
- [40] W. Press, S. Teukolsky, W. Vetterling, and B. Flannery, *Numerical Recipes in C - The Art of Scientific Computing (2nd Edition)* (Cambridge University Press, [http://www.ulib.org/webRoot/Books/Numerical\\_Recipes/](http://www.ulib.org/webRoot/Books/Numerical_Recipes/), 1997).
- [41] Not exactly, because of equation B3.